Research Paper

Remote loading of liposomes with a ^{124}I-radioiodinated compound and their *in vivo* evaluation by PET/CT in a murine tumor model

Gokce Engudar[1,5], Henrik Schaarup-Jensen[1,5], Frederikke P. Fliedner[2], Anders E. Hansen[2,3,5], Paul Kempen[3,5], Rasmus I. Jølck[3,5], Andreas Kjaer[2], Thomas L. Andresen[3,5], Mads H. Clausen[1,5], Andreas I. Jensen[4,5], Jonas R. Henriksen[3,5][⊠]

1. Department of Chemistry, Technical University of Denmark, 2800 Lyngby, Denmark.
2. Cluster for Molecular Imaging, Dept. of Biomedical Sciences and Dept. of Clinical Physiology, Nuclear Medicine & PET, Rigshospitalet and University of Copenhagen, 2200 Copenhagen.
3. Department of Micro- and Nanotechnology, Technical University of Denmark, 2800 Lyngby, Denmark.
4. Center for Nuclear Technologies, Technical University of Denmark, 4000 Roskilde, Denmark.
5. Center for Nanomedicine and Theranostics, Denmark.

*Corresponding author: Jonas R. Henriksen, jhen@nanotech.dtu.dk

⊠ Corresponding author:

Abstract

Long circulating liposomes entrapping iodinated and radioiodinated compounds offer a highly versatile theranostic platform. Here we report a new methodology for efficient and high-yield loading of such compounds into liposomes, enabling CT/SPECT/PET imaging and ^{131}I-radiotherapy.

Methods: The CT contrast agent diatrizoate was synthetically functionalized with a primary amine, which enabled its remote loading into PEGylated liposomes by either an ammonium sulfate- or a citrate-based pH transmembrane gradient. Further, the amino-diatrizoate was radiolabeled with either ^{124}I ($t_{1/2}$ = 4.18 days) for PET or ^{125}I ($t_{1/2}$ = 59.5 days) for SPECT, through an aromatic Finkelstein reaction.

Results: Quantitative loading efficiencies (>99%) were achieved at optimized conditions. The ^{124}I-labeled compound was remote-loaded into liposomes, with an overall radiolabeling efficiency of 77 ± 1%, and imaged *in vivo* in a CT26 murine colon cancer tumor model by PET/CT. A prolonged blood circulation half-life of 19.5 h was observed for the radiolabeled liposomes, whereas injections of the free compound were rapidly cleared. Lower accumulation was observed in the spleen, liver, kidney and tumor than what is usually seen for long-circulating liposomes.

Conclusion: The lower accumulation was interpreted as release of the tracer from the liposomes within these organs after accumulation. These results may guide the design of systems for controlled release of remote loadable drugs from liposomes.

Key words: remote loading, pH-gradient liposomes, transmembrane ammonium sulfate, iodinated imaging agents, I-124, PET imaging

Introduction

Nanoparticles and liposomes in particular, have been vigorously investigated due to their ability to improve the biodistribution of small molecular drugs. The multifunctional nature of liposomes has furthermore potentiated their use as theranostic agents and companion diagnostics [1]. Here, diagnostic liposomes are used for initial patient screening, while their therapeutic counterparts are used in follow-up treatment [2,3]. The prolonged blood circulation and enhanced tissue accumulation

of liposomes have also precipitated their use in imaging of the hepatic and cardiovascular systems [4], and for clinical and preclinical assessment of the enhanced permeation and retention (EPR) effect in tumors [5,6]. Alternative compositions such as nanoemulsions, micelles, polymeric and metal alloy nanoparticles are also being explored as reporters of the EPR effect [7–9]. Several imaging modalities have been used in combination with liposomes for diagnostic purposes, including gadolinium-based magnetic resonance imaging (MRI), [99mTc] and [111In] for single photon emission computed tomography (SPECT), [64Cu], [89Zr], [52Mn] and [18F] for positron emission tomography (PET) and iodine for X-ray computed tomography (CT) [4,5,10–19].

Iodine has 37 isotopes and covers most of the above-mentioned modalities. Non-radioactive iodine ([127I]) is radiodense and provides contrast in radiographic imaging agents, while various iodine radioisotopes are applied in molecular imaging for SPECT ([123I], [125I] and [131I]) and PET ([124I]). Iodine radioisotopes are further used as radioactive tracers in surgical guidance [20,21], and for internal radiotherapy via beta irradiation ([131I]), photon irradiation ([125I]) and more recently in Auger therapy ([125I]) [22]. In recent years, [124I] ($t_{1/2}$ = 4.18 days) has gained particular attention as a long-lived radioisotope for PET imaging. [124I] has a positron branch of 23% ($E_{average}$ = 686 keV (11%) and 974 keV (11%)) as well as several high-energy gamma emissions (511 keV (46%), 603 keV (61%), 723 keV (10%) and 1691 keV (11%) [23]. Recent phase I/II studies have demonstrated [124I] to be a valuable theranostic agent supporting current clinical [131I] treatments of differentiated thyroid cancer, by improving staging, grading and lesion delineation using PET imaging [24]. Taking advantage of the well-established iodine radiochemistry, labeling procedures can easily be adapted for each radioisotope. This gives access to either SPECT, PET or CT modalities for imaging and low-energy beta particle therapy [25]. The combination of iodine and liposomes thus offers a highly versatile theranostic platform.

Visualization of the blood pool and tumor vasculature has previously been investigated using liposomes labeled with iodine or radioiodine through either: i) passive encapsulation, ii) membrane incorporation of chemically modified iodo-lipids, or iii) remote-loading of iodine-rich species [4,26,27]. Passive encapsulation, however, suffers from low encapsulation efficiencies and laborious preparation procedures [28–31], while remote loading of liposomes using the well-known Bolton-Hunter reagent offers iodine loading efficiencies of only about 60% [32]. Accordingly, there is an unmet need to develop new methods for loading iodinated compounds into liposomes with quantitative loading efficiencies.

Transmembrane chemical potentials across lipid bilayers created by ion gradients can be used as a driving force for loading compounds into liposomes with high efficiency, as previously demonstrated for the clinically approved formulation Doxil™ [33–36]. In recent studies, similar approaches were applied to load radionuclides, such as the single photon emitter [99mTc], the therapeutic radioisotope [186Re] and positron emitters [64Cu] and [52Mn] [10,13,17,37–39].

In the present study, we report a new method for loading liposomes with an iodine-rich compound (**Figure 1**). Diatrizoic acid, an iodinated CT contrast agent used clinically for visualization of, e.g., the bowel [40] and in digital subtraction angiography [41], was functionalized to carry a primary amine, enabling its remote loading into liposomes by a transmembrane pH gradient. While the unprotonated species may traverse the lipid membrane, protonation inside the liposome serves to trap it there. Remote loading was accomplished using either citrate- or ammonium sulfate-based pH gradients, and was further optimized by varying the pH of the utilized buffers, the compound-to-lipid ratio, and the duration of the loading procedure. [124I] radioiodinated diatrizoic acid analogues were obtained by an aromatic Finkelstein reaction [42], and were remote loaded into stealth liposomes. The biodistribution of the [124I]-radiolabeled stealth liposomes and the free compound was evaluated by PET/CT imaging and *ex vivo* gamma counting in tumor-bearing mice. Radiolabeling of liposomes with [125I] via remote loading was furthermore conducted as part of the optimization procedure.

Such iodine-loaded liposomal theranostic agents are highly valuable for future biomedical applications, including diagnosis and staging of disease and for evaluation of therapeutic responses.

Methods

Materials

For synthesis of the imaging agent, starting materials, reagents and solvents were purchased from commercial suppliers and used without further purification. All solvents beside 2-methoxy-ethanol were HPLC grade and dry solvents were obtained via an Innovative Technology PS-MD-7 puresolv system. [[124I]]NaI and [[125I]]NaI were purchased from PerkinElmer Life Science as solutions in aqueous NaOH (0.02 M and 10^{-5} M, respectively).
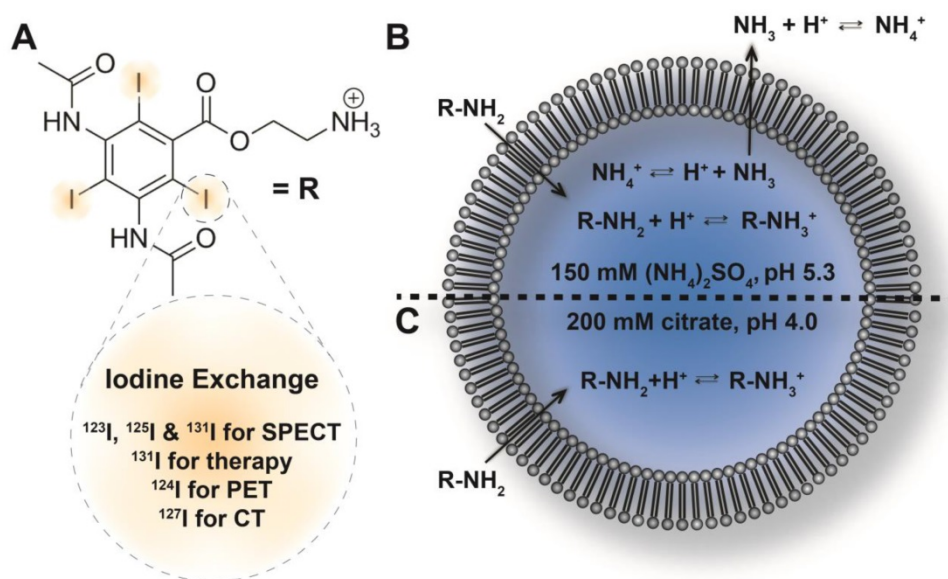
Figure 1. Remote loading of the amino diatrizoic acid (ADA) imaging agent **(A)** into liposomes by transmembrane pH gradients. Possible iodine labels for SPECT, therapy, PET and CT are outlined. Equilibria governing the remote loading of amine-functionalized compounds into liposomes via ammonium sulfate-based **(B)** or citrate-based **(C)** pH gradients are shown.

The lipid mixture, composed of hydrogenated soy L-α-phosphatidylcholine (HSPC), cholesterol (CHOL) and 1,2-distearoyl-*sn*-glycero-3-phosphoethanolamine-N-[methoxy(polyethylene glycol)-2000] (ammonium salt) (DSPE-PEG$_{2000}$) in the molar ratio HSPC:CHOL:DSPE-PEG$_{2000}$ (56.5:38.2:5.3), was purchased from Lipoid GmbH. 1,2-dipalmitoyl-*sn*-glycero-3-phosphoethanolamine-N (lissamine rhodamine B sulfonyl) (ammonium salt) (Rho-DPPE) was purchased from Avanti Polar Lipids. Reagents used in the ICP-MS experiments, nitric acid and tetramethylammonium hydroxide solution (25% in H$_2$O), were TraceSelect® and purchased from Fluka Analytical and Te, Ga, P standards and potassium iodide were purchased from Sigma-Aldrich. Ammonium sulfate, citric acid, trisodium citrate dihydrate, sodium phosphate monobasic dihydrate, sodium phosphate dibasic dihydrate, sodium chloride, sodium carbonate, HEPES ([4-(2-hydroxyethyl)-piperazino]-1-ethanosulfonic acid) and HEPES sodium salt, Trizma®base (tris(hydroxymethyl)aminomethane), MES (2-(*N*-morpholino) ethanesulfonic acid), and CHES (2-(cyclohexylamino)ethanesulfonic acid), were purchased from Sigma-Aldrich. Water used for all experiments was collected from a Milli-Q system (Millipore).

Illustra™ MicroSpin™ G-50 columns and PD-10 desalting columns were from GE Healthcare. Slide-A-Lyzer® 10k Dialysis Cassettes were from ThermoScientific. Amicon® Ultra (4 and 0.5 mL; 30k and 100k) centrifugal filter devices were purchased from Millipore. Sep-Pak® Plus Silica cartridges (690 mg sorbent per cartridge, 55-105 μm particle size)

were purchased from Waters. TLC plates (Silica gel 60 F$_{254}$) were purchased from Merck.

An isotonic HEPES buffer (25 mM HEPES, 150 mM NaCl) was prepared by mixing HEPES and HEPES sodium salt in Milli-Q water and adjusted to pH 7.4 with HCl (osmolality: 310 mOsm/kg). Phosphate buffer was prepared by mixing sodium phosphate monobasic dihydrate and sodium phosphate dibasic dihydrate to obtain pH 7.0 (25 mM phosphate, 150 mM NaCl, pH 7.0, 326 mOsm/kg). CHES buffer (25 mM CHES, 150 mM NaCl, pH 9.0, 310 mOsm/kg), MES buffer (25 mM MES, 150 mM NaCl, pH 6.0, 307 mOsm/kg) and TRIS buffer (25 mM TRIS, 150 mM NaCl, pH 8.0, 313 mOsm/kg) were prepared in Milli-Q water and the pH values were adjusted with HCl/NaOH to desired pH. Sodium citrate buffer was prepared by mixing citric acid and trisodium citrate dihydrate for the final pH of 4.0 (200 mM citrate, pH 4.0, 380 mOsm/kg).

Synthesis of amino diatrizoic acid (ADA)

Diatrizoic acid **1** was esterified by nucleophilic substitution of 2-(boc-amino)ethyl bromide (1.5 equiv.) in DMF at 50 °C by forming the corresponding carboxylate of **1** using K$_2$CO$_3$ (1.2 equiv). This afforded the ester **2** in fair yield (48%). The Boc-group of **2** was subsequently removed using TFA in CH$_2$Cl$_2$ yielding the TFA salt of **3** in quantitative yield (For detailed synthetic procedures and NMR spectra of final product, see Supporting Information data S1). Compound **3** is hereafter referred to as amino diatrizoic acid (ADA).
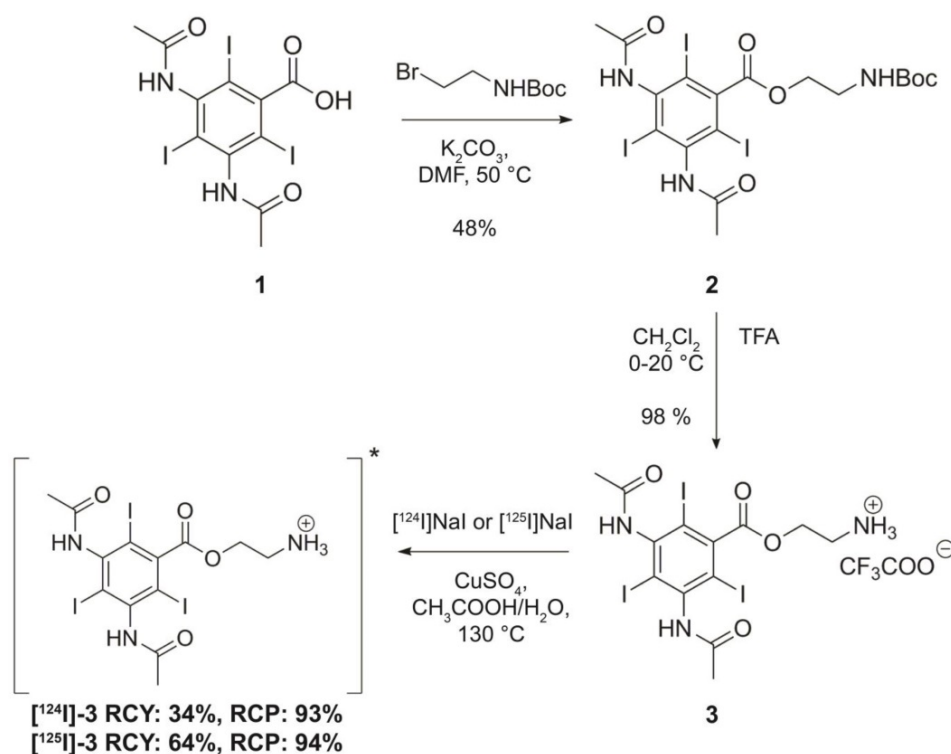
Scheme 1. Synthetic scheme of amino-functionalized diatrizoic acid **(3)** and radioiodination.

Synthesis of [^{124}I]ADA and [^{125}I]ADA

[^{124}I]ADA and [^{125}I]ADA were synthesized using an aromatic Finkelstein reaction (iodine-iodine exchange) modified from Aissi et al [42]. Amino diatrizoic acid (ADA) (0.35 mg, 0.45 µmol, TFA salt) was dissolved in glacial acetic acid (240 µL) in a glass vial, followed by adding a dispersion of CuSO$_4$ in glacial acetic acid (120 µL, 1.0 mg/mL, 0.76 µmol). [^{124}I]NaI as an aqueous solution in 0.02 M NaOH (120 µL, 109 MBq) was added and the mixture was magnetically stirred in a closed vial at 130 °C for 2.5 h. After cooling to ambient temperature, ethyl acetate (720 µL) was added to the mixture and the resulting solution was applied to a Sep-Pak Plus Silica cartridge. The product was subsequently isolated by sequential elution of 10 fractions (F) according to the following scheme: F1: neat ethyl acetate (3 mL), F2: EtOH:EtOAc:AcOH (75:25:1) (2 mL), F3: EtOH:EtOAc:AcOH (90:10:1) (1 mL), F4: EtOH:EtOAc (90:10) (1 mL), F5: EtOH:25% aq. NH4OH (99:1) (1 mL), F6: EtOH:25% aq. NH$_4$OH (98:2) (1 mL), F7: EtOH:25% aq. NH4OH (97:3) (1 mL), F8: EtOH:25% aq. NH4OH (96:4) (1 mL), F9: EtOH:25% aq. NH$_4$OH (95:5) (1 mL), F10: EtOH:25% aq. NH$_4$OH (95:5) (1 mL). Fractions 5-10 were pooled and evaporated to dryness at 70 °C under a stream of air for 35 min, furnishing the desired product. Likewise, to radiolabel ADA with ^{125}I, ADA (1.0 mg, 1.3 µmol, TFA salt) was dissolved in glacial acetic acid (100 µL) and a dispersion of CuSO$_4$ in glacial acetic acid was added (100 µL, 1.0 mg/mL, 0.63 µmol). An aqueous solution of [^{125}I]NaI in 10^{-5} M NaOH (3 µL, 8.7 MBq) and water (7 µL) was added to this mixture. The resulting solution was magnetically stirred at 130 °C for 30 min. After cooling to room temperature, ethyl acetate (400 µL) was added to the mixture. The product was isolated using a Sep-Pak Plus Silica cartridge and sequential elution in accordance with the above gradient scheme. Fractions F5-10 were evaporated to dryness at 60 °C under a stream of air for 45 min.

Preparation of liposomes with a transmembrane ammonium gradient

The lipid mixture composed of HSPC:CHOL:DSPE-PEG$_{2000}$ (56.5:38.2:5.3 molar ratio) was mixed with Rho-DPPE in a tert-butanol:water (9:1) (0.2 mol% fluorescent lipid), and lyophilized overnight. Rhodamine B was included for UV-VIS detection of these liposomes. The freeze-dried lipid was hydrated in 150 mM ammonium sulfate (pH 5.3, 330 mOsm/kg) for 1 h at 65 °C and seven freeze-thaw cycles were conducted before sizing to large unilamellar vesicles (LUVs). To form LUVs, the liposome suspension was extruded through either 200 nm or 100 nm (for the in vivo PET study) pore sized polycarbonate membranes by an Avanti mini extruder at 65 °C. The hydrodynamic diameter and size distribution of the liposomes were determined by dynamic light scattering (ZetaSizer, Malvern

Instruments) and the phosphorous content by ICP-MS (iCAP Q, Thermo Scientific).

The ammonium sulfate gradient was created using Slide-A-Lyzer® 10K Dialysis Cassettes (buffer volume was 300-fold the volume of the sample) for buffer exchange with buffers having different pH values. The dialysis buffer was replaced three times with new buffer to provide a successful buffer exchange. The external buffers were isotonic 25 mM phosphate buffer pH 7.0, TRIS pH 8.0, CHES pH 9.0 or MES pH 6.0 buffers all containing 150 mM NaCl. The average hydrodynamic diameter of the liposomes was 146 nm (PDI: 0.062).

Preparation of liposomes with a citrate based transmembrane pH gradient

Large unilamellar vesicles (LUVs) were prepared as previously described using a 200 mM sodium citrate buffer ($C_6H_8O_7$: $Na_3C_6H_5O_7$, pH 4.0, 380 mOsm/kg) for hydration. The liposome solution was incubated for 1 h at 65 °C, followed by seven freeze-thaw cycles. The transmembrane pH gradient was formed by increasing the external pH of liposomes to a desired pH of 7.0 by adding aq. sodium carbonate (1 M, pH 11.8), resulting in a final lipid concentration of 50 mM (volume ratio of base and liposomes $V_{base}/V_{liposome}$ = 0.2). The hydrodynamic diameters of the liposomes extruded through 200 nm or 100 nm filters were 142 nm (PDI = 0.072) or 137 (PDI = 0.042) respectively.

Remote loading and quantification of ADA and [124I]ADA

Having formed the ion gradient across the liposome membrane, the liposome dispersion was added to solid ADA. As an example, 2.2 mg ADA (2.9 µmol) was mixed with aq. 550 uL liposomes (50 mM lipid). For the ammonium sulfate gradient liposomes, a fixed ADA-to-lipid molar ratio of 0.1 was used for the method optimization in combination with varying the external pH (6-9) and incubation time (1-24 h). For the citrate gradient liposomes, ADA-to-lipid ratios from 0.1 to 1.0 were investigated at constant lipid concentration and as a function of the incubation time (1-24 h). Initial screening revealed 55 °C to be the optimal incubation temperature when judged by loading rate (data not shown). All samples were heated and continuously stirred at 55 °C.

Quantification of the liposome loading efficiency of ADA

The loading efficiency was quantified as the ratio of the ADA-to-lipid ratio before and after microcolumn separation of the free and liposome entrapped ADA. Briefly, a 25 µL liposome sample was applied to the Illustra MicroSpin G-50 columns (GE Healthcare) and centrifuged at 2000 ×g for 4 min. The ADA-to-lipid ratio (before and after column separation) was determined by UV-VIS spectroscopy (NanoDrop 2000C, ThermoScientific), where rhodamine labeled DPPE acted as a surrogate for the full lipid sample. Samples with ADA-to-lipid ratio of 0.1, 0.25, 0.5 or 1.0 were diluted either 150, 300, 600 or 1200-fold in ethanol containing 0.6 v/v % TFA respectively, prior to the UV-VIS measurement in order to dissolve the liposomes and assure protonation of ADA. The absorbance of ADA and Rho-DPPE (liposomes) were measured at 243 nm (λ_{max}) and 560 nm (λ_{max}) respectively, and the loading efficiency was calculated as (**Equation 1**):

$$\% \, LE = \frac{A_{243,a}}{A_{560,a}} \cdot \frac{A_{560,b}}{A_{243,b}} \cdot 100\%$$

where $A_{243,b}$ and $A_{243,a}$ denote the peak absorbance of ADA before and after column separation respectively. $A_{560,b}$ and $A_{560,a}$ denote the peak absorbance of Rho-DPPE (liposome) before and after column separation respectively (**Figure S3** and **Figure S4**).

Iodine and phosphor concentrations of the liposomes were in addition quantified by ICP-MS (Thermo Scientific, iCAP Q) to verify the loading efficiency determined by UV-VIS spectroscopy (**Figure S5**).

Preparation of [124I]ADA in HEPES buffer for *in vivo* study

Radiolabeled [124I]ADA (45.3 MBq, 1.2 µmol) was dissolved in EtOH:H_2O (7:1, 800 µL). From this solution, 110 µL (5.24 MBq) was evaporated to dryness under argon flow for 5 min at 70 °C. The residue was redissolved in isotonic HEPES buffer (500 µL) and used directly for the in vivo study. The final activity concentration was 9.0 MBq/mL at the time of injection.

Preparation of [124I]ADA loaded liposomes for *in vivo* study

Citrate-based transmembrane pH gradient liposomes for the *in vivo* study were prepared as described above, resulting in liposomes with hydrodynamic diameters of 137 nm (PDI = 0.04). Radiolabeled [124I]ADA (45.3 MBq, 1.2 µmol) was dissolved in EtOH:H_2O (7:1, 800 µL), whereafter 39 MBq (690 uL) was transferred to an HPLC vial and evaporated to dryness under argon flow for 5 min at 70 °C. Citrate-based transmembrane pH gradient liposomes (50 mM, 510 µL) were added to the dry [124I]ADA (39 MBq) and incubated for 3 h at 55 °C with continuous stirring. The initial ADA-to-lipid

molar ratio was 0.04. After loading, non-encapsulated [124I]ADA and external citrate buffer were removed by exchanging the external medium with HEPES buffer (25 mM, 150 mM NaCl, pH 7.4, 310 mOsm/kg) using PD-10 desalting columns (GE Healthcare). The final lipid and activity concentration of the collected liposomes were 10.2 mM and 20.5 MBq/mL at the time of injection.

Quantification of the [124I]ADA loading efficiency

[124I]ADA-loaded liposomes and free [124I]ADA were separated using PD-10 desalting columns (GE Healthcare). The sample was applied to the column and 500 µL fractions were collected by eluting with isotonic HEPES buffer. The radioactivity of the collected fractions was measured using a dose calibrator (CRC-55tR, Capintec, Inc.). The loading efficiency was calculated as the ratio of the radioactivity of 124I in the liposome fraction to the total radioactivity in the collected fractions. Furthermore, the PD-10-purified 124I-liposomes were analyzed by thin-layer chromatography (TLC) in order to determine the radiochemical purity. 2 µL of purified [124I]ADA-liposomes were spotted on a TLC plate (Silica gel 60 F_{254}) and ethanol:25% aq. NH_4OH (99:1) was used as eluent. The radio-TLC was measured using a phosphor imager (Cyclone Plus, PerkinElmer) and the [124I]ADA compound was identified at Rf = 0.35, which was identical to the non-radioactive reference (ADA).

Cryo-TEM imaging

3 µL of liposome solution was placed on a lacy carbon 300 mesh copper TEM grid, blotted and plunge frozen in liquid ethane using a FEI Vitrobot Mark IV. Samples were imaged using a FEI Tecnai G2 20 TWIN transmission electron microscope operated at 200 keV in low-dose mode with a FEI High-Sensitive (HS) 4k × 4k Eagle camera.

Animal model

Tumors were established by subcutaneous injection of 3×10^5 CT26 murine colon cancer cells (CRL-2638, American Type Culture Collection, ATCC, VA, USA) suspended in 100 µL of culture medium over the thigh/flank of 7-week-old female BALB/c mice (Janvier Labs, France). Cells were grown in vitro in culture flasks using RPMI medium (Gibco, Thermo Fisher, Waltham, Massachusetts, USA) supplemented with bovine serum albumin (Gibco, Thermo Fisher, Waltham, Massachusetts, USA) and Penicillin Streptomycin (Pen Strep, (Gibco, Thermo Fisher, Waltham, Massachusetts, USA)) before inoculation in mice. Cells were tested for murine virus, human virus, mycoplasma, and lastly tested for cell line

authentication to exclude cross-contamination during in vitro growth. Tumors were allowed to grow for 16 days before study start. The National Animal Experiments Inspectorate approved all study procedures (license no. 2016-15-0201-00920).

MicroPET/CT imaging procedure

PET/CT imaging was performed on an Inveon® small animal PET/CT system (Siemens Medical Systems, PA, USA). Mice were anesthetized by inhalation of anesthesia (~3% sevoflurane) and either 3.46 ± 0.04 MBq/mouse of [124I]ADA -liposomes (n = 5) or 1.39 ± 0.05 MBq/mouse of [124I]ADA in HEPES (n = 3) was injected into the tail vein. The mice receiving liposomes were each administered 1.3 mg lipid and 71 µg ADA, whereas the mice administered the free compound received 29 µg ADA each. Decay-corrected injected activities were determined by gamma counting syringes before and after injections. [124I]ADA -liposomes or [124I]ADA was allowed to distribute for 18 min before commencing a 5 min PET scan (Scan1) and a corresponding CT scan. Additional PET/CT scans were performed after a distribution period of 1.5 h (Scan2) (5-min acquisition), 20 h (Scan3) (10-min acquisition), 48 h (Scan4) (15-min acquisition) and 70 h (Scan5) (15-min acquisition). Emission data were corrected for dead time and decay and attenuation correction was performed based on the corresponding CT scan. PET scans were reconstructed using a maximum a posteriori (MAP) reconstruction algorithm (0.815×0.815×0.796 mm). Image analysis was performed using Inveon® software (Siemens Medical Systems, PA, USA). 3D regions of interest (ROIs) were manually constructed and decay-corrected data (%injected dose per gram tissue (%ID/g)) are reported.

Gamma counting

For post mortem analysis, the following tissues were collected and transferred into pre-weighed gamma counter tubes: blood, liver, spleen, kidney, tumor and thyroid gland (complete larynx region). All tubes were well counted using an 124I setup and decay corrected (Wizard gamma counter, Perkin Elmer, Waltham, MA. USA). The specific activity is reported as %ID/g and is based on the total injected activity and the measured activity and weight of the tissue samples. The activity of the thyroid gland was determined from the overall activity in the excised complete larynx region, which was not further dissected to avoid damaging the thyroid. The measured activity was assumed to be primarily from the thyroid gland and activity is therefore reported as injected dose in the thyroid gland (%ID/thyroid).

Results and Discussion

Synthesis and characterization of ADA

A diatrizoic acid derivative (ADA) was synthesized by esterification with 2-(boc-amino)ethyl bromide. This introduced an amino group to enable remote loading into liposomes via a transmembrane pH gradient. The pKa value of the primary amine on ADA was determined to be 8.56 ± 0.04 (n = 4) by acid-base titration and LogD values of -0.6 (pH 5) and 0.6 (pH 7.4) were estimated using the ChemAxon software package (**Figure S1** and **Figure S2**). The pKa and corresponding change in hydrophilicity upon protonation of the amine allows ADA to traverse lipid membranes at neutral pH but not at lower pH values. This makes ADA suitable for remote-loading into the liposomes.

Optimizing the remote loading of ADA into liposomes

Remote loading of ADA into stealth liposomes was conducted using either an ammonium sulfate- or a citrate-based pH gradient method. A Rho-DPPE lipid fluorophore was included to enable quantification of the lipid fraction. The loading efficiency could therefore be determined by UV-VIS spectrophotometry (**Figure 2A**), via the absorbance of ADA at 243 nm and Rho-DPPE at 560 nm. By use of **Equation 1**, the loading efficiency, %LE, was determined via the ADA-to-lipid ratio before and after removal of non-loaded ADA by spin column separation (see **Figure S3** and **Figure S4** for UV-VIS spectra of ADA and liposomes used for quantification of the loading efficiencies). Iodine and phosphor concentrations of several UV-VIS samples were in addition quantified by ICP-MS for verification of the method (**Figure S5**). For both sets of liposomes, dry ADA solids were stirred directly with the liposomes,
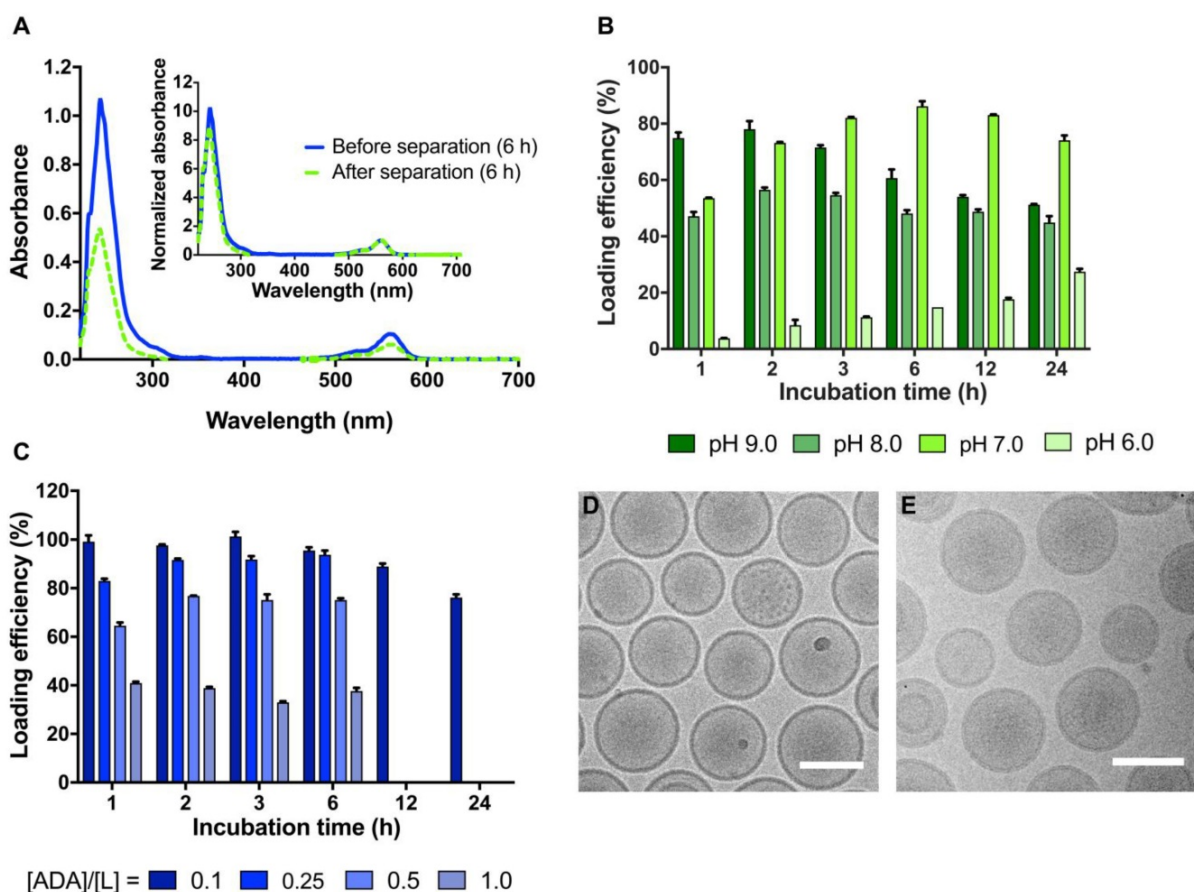

Figure 2. Remote loading of non-radioactive ADA into liposomes via transmembrane ammonium sulfate or citrate pH gradients. **(A)** UV-VIS spectra of ADA-loaded liposomes before and after removal of free ADA by MicroSpin column separation. Inset: normalized UV-VIS spectra where the absorbance of Rho-DPPE at 560 nm has been set to unity. The normalized spectrum enables direct comparison of the ADA-to-lipid ratio before and after removal of non-loaded ADA by spin column separation. **(B)** The loading efficiency of ADA into ammonium sulfate gradient liposomes is shown as a function of time and external pH. The loading experiments were conducted at a 0.1 ADA-to-lipid molar ratio and at 55 °C. **(C)** The loading efficiency of ADA into citrate gradient liposomes is shown as a function of the ADA-to-lipid ratio and time. The loading experiments were conducted at 55 °C with an external pH of 7.0. **(D)** Cryo-TEM images of ADA-loaded ammonium sulfate liposomes with an ADA-to-lipid ratio of 0.2. **(E)** Cryo-TEM images of ADA-loaded sodium citrate liposomes with an ADA-to-lipid ratio of 0.2. The scale bars are 100 nm.

and all reported loading efficiencies describe the combined process of initial dissolution and subsequent loading of ADA into the liposomes. Both solubility and membrane permeation are highly dependent on the overall charge of ADA and thereby dependent of the pH outside the liposomes. An optimal pH of 7.0 was identified for the ammonium sulfate gradient liposomes (at 55 °C and 0.1 ADA-to-lipid ratio), yielding a maximal loading efficiency of 86 ± 2% after 6 h of stirring, followed by a 12% decline in the loading efficiency at 24 h (**Figure 2B**). Liposomes with an external pH of 6.0 exhibited the lowest loading efficiencies, reaching a maximal loading of 27 ± 1% after 24 h of stirring (**Figure 2B**). The reduced loading efficiency at pH 6.0 is likely caused by poor membrane permeation of the protonated ADA species leading to slow loading kinetics. At external pH 8.0 and 9.0, the maximal loading efficiency was reached at 2 h, yielding 56 ± 1% and 78 ± 3% respectively (**Figure 2B**). The reduction in loading efficiency obtained at pH 8.0 and 9.0 compared to pH 7 may be explained by lower solubility and/or slow dissolution kinetics of the dry ADA at higher external pH values due to limited protonation. Further studies are required to determine the exact cause of the reduced loading efficiency found at pH 6, 8 and 9 compared to pH 7.

Having identified an optimal external pH of 7.0, citrate gradient-based liposomes were investigated. These liposomes were prepared in citrate buffers with an internal lumen pH of 4.0, and an external pH of 7.0. This procedure utilizes the polyprotic nature of citrate, and provides an instant pH gradient across the liposome membranes in a quick and simple manner. Using this method, concentrated liposome samples (50 mM lipid) were prepared with membrane gradients of $\Delta pH = 3.0$, without any purification steps and with limited sample dilution (~20% upon addition of sodium carbonate). Such liposomes of high lipid concentration and simple gradient formation are highly warranted when large compound payloads are desired. In order to determine the maximal payload of ADA into the citrate-based liposomes, the loading efficiency was determined for the ADA-to-lipid molar ratios 0.1, 0.25, 0.5 and 1.0. For all ADA-to-lipid molar ratios, the loading efficiency remained approximately constant at the 1, 2, 3 and 6 h time-points, beyond which a slight decrease in loading efficiency was observed for the 0.1 ADA-to-lipid ratio (**Figure 2C**). This decrease in loading efficiency after 12-24 h incubation may be governed by slow dissipation of the citrate pH gradient, resulting in unloading of the ADA compound. Similar observations have been reported by Forster et al [43]. Loading efficiency levels of 98 ±

1%, 90 ± 2%, 73 ± 3% and 38 ± 2% were obtained at ADA-to-lipid ratios of 0.1, 0.25, 0.5 and 1.0 respectively, demonstrating that the citrate pH gradient is gradually exhausted as more ADA compound is loaded into the core of the liposomes. This observation is in accordance with previous reports [44]. The effectively entrapped payload of ADA per liposome, given as the product of the loading efficiency and the ADA-to-lipid molar ratio, increases from [ADA]/[Lipid] = 0.098, 0.23, 0.37 to 0.38 for ADA-to-lipid molar ratios 0.1, 0.25, 0.5 and 1.0 respectively. The effective entrapped payload thus converges towards [ADA]/[Lipid] = 0.38, which corresponds to 14.5 mg iodine/mL for a 100 mM lipid solution. Hence, production of long-circulating high CT contrast liposomes by remote loading using the current approach seems to not be feasible, as 50-200 mg/mL iodine is often required to obtain significant CT contrast levels [4,31]. Improved payloads of iodine in liposomes may still be obtained by entrapping higher citrate concentrations and/or utilizing liposomes with increased diameter. However, such changes impact the osmotic transmembrane gradient and systemic circulation properties of the liposome [45]. Cryo-TEM images of citrate and ammonium sulfate gradient liposomes loaded with ADA are shown in **Figure 2D-E**, displaying populations of spherical monodisperse liposomes in both cases. Neither the citrate- nor ammonium sulfate-based liposomes were found to entrap visible precipitates of ADA at an ADA-to-lipid ratio of 0.2, such as is found in Doxil where crystals of doxorubicin are present after remote loading [46,47].

Radiolabeling of ADA with [124]I and [125]I

[124]I substitution of iodine on ADA was conducted using a modified Cu(I)-catalyzed nucleophilic isotopic exchange reaction (**Scheme 1**) [42]. The radiochemical purity of the purified [[124]I]ADA was >90%, with a radiochemical yield of 34-55% and a specific activity of 83 MBq/µmol. ADA was in addition radiolabeled with ^{125}I through a 30 min reaction, which resulted in a radiochemical purity of 94% and a higher purified radiochemical yield of 64%. Since [124]I could only be acquired in lower concentration than ^{125}I, it was necessary to conduct the radiolabeling with this radionuclide at higher water concentrations. This was observed to drastically lower the reaction rate, which made it necessary to extend the reaction time. This led to an increased presence of impurities and lowered radiochemical yields for the [124]I radiolabeling. Radiochemical conversion (not purified) for similar reaction conditions on an ortho-iodinated benzyl group has previously been reported to be around 75-82% after 30 min of reaction,

with a slight drop to around 70% after 45 min [42]. Accordingly, our RCYs and conversion for ^{125}I are on par with reported values and the extended reaction time may compromise yields, likely due to harsh reaction conditions. The reaction used is theoretically applicable to all isotopes of iodine, but as was observed, the concentration and manner in which an isotope can be acquired may affect practical procedures.

Remote loading of [[124]I]ADA and [^{125}I]ADA into liposomes

For remote loading of the radiolabeled analogue of ADA, liposomes entrapping citrate were chosen due to their higher loading efficiency and faster loading kinetics (**Figure 2B-C**) when compared to their ammonium sulfate counterparts. The longer-lived [^{125}I]ADA analogue was used for the initial optimization of the radio-TLC and PD-10 size exclusion column analyses, as well as for the test loading of liposomes. Subsequently, the [[124]I]ADA analogue was synthesized for evaluation of the liposome biodistribution in mice by PET/CT imaging and organ well counting. The average radiochemical purity of [^{125}I]ADA and [[124]I]ADA was $93.0 \pm 0.6\%$ (n = 4) when assessed by radio-TLC (**Figure S6**). However, remote loading of both [^{125}I]ADA and [[124]I]ADA, with subsequent size exclusion purification, resulted in radiochemical purities of more than 99% (**Figure 3B**) in all cases. We believe this to be a result of only the target compound (ADA) undergoing remote loading, whereas other small-molecular radioactive impurities were removed by the PD-10 purification. The average loading efficiency was $77 \pm 1\%$ (n = 4) when assessed by PD-10 column separation (**Figure 3A**). Overall, this

correspond to 84% of the loadable activity being entrapped in the liposomes, which is a 30% improvement compared to the Bolton-Hunter reagent method reported by Mougin-Degraef et al [32].

For the *in vivo* studies, the liposome sample was purified on a PD-10 column, with concomitant exchange of the medium from hypertonic citrate (380 mOsm/kg) to isotonic HEPES buffer. After column separation, citrate gradient liposomes were collected with lipid and radioactivity concentrations of 10.2 mM and 20.5 MBq/mL respectively at the time of injection. The loading efficiency after column purification was 98%. The stability of the encapsulation of the loaded radiotracer was assessed by incubating the [[124]I]ADA liposomes at 25 °C for 168 h in HEPES buffer. This resulted in an encapsulation efficiency of $98 \pm 1\%$ (n = 3), testifying to the excellent stability of this loading method.

In vivo evaluation of [[124]I]ADA loaded liposomes

[[124]I]ADA and [[124]I]ADA liposomes were well tolerated by all mice and no reactions to the injections or during the observation period were seen. Representative MIP and axial PET/CT images are shown in **Figure 4** (see **Figure S8** for sagittal and coronal PET/CT images). Biodistributions of free and liposome-loaded [[124]I]ADA in CT26 tumor-bearing mice at each time-point were determined from the PET scans (**Figure 5A-E**). The biodistributions were further verified by gamma counting organs including the thyroid regions after a distribution period of 72 h (**Figure 5F-G**).
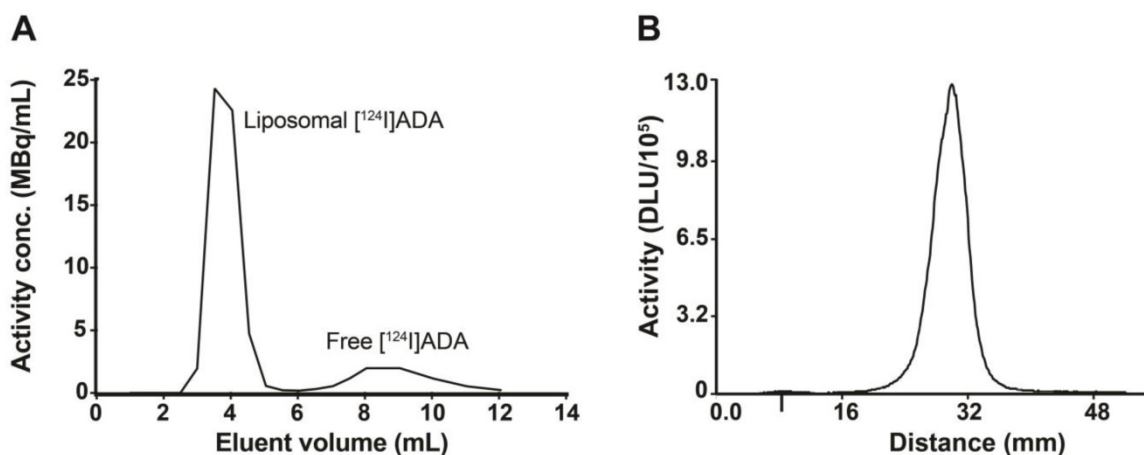

Figure 3. Characterization of [[124]I]ADA loaded liposomes by size exclusion column separation and radio-TLC. **(A)** Elution profile of [[124]I]ADA-loaded liposomes by PD-10 column separation. The liposomes were eluted with 25 mM HEPES buffer (150 mM NaCl, pH 7.4, 310 mOsm/kg), with a loading efficiency of 77.2%. **(B)** Radio-TLC peak of [[124]I]ADA after loading into liposomes.
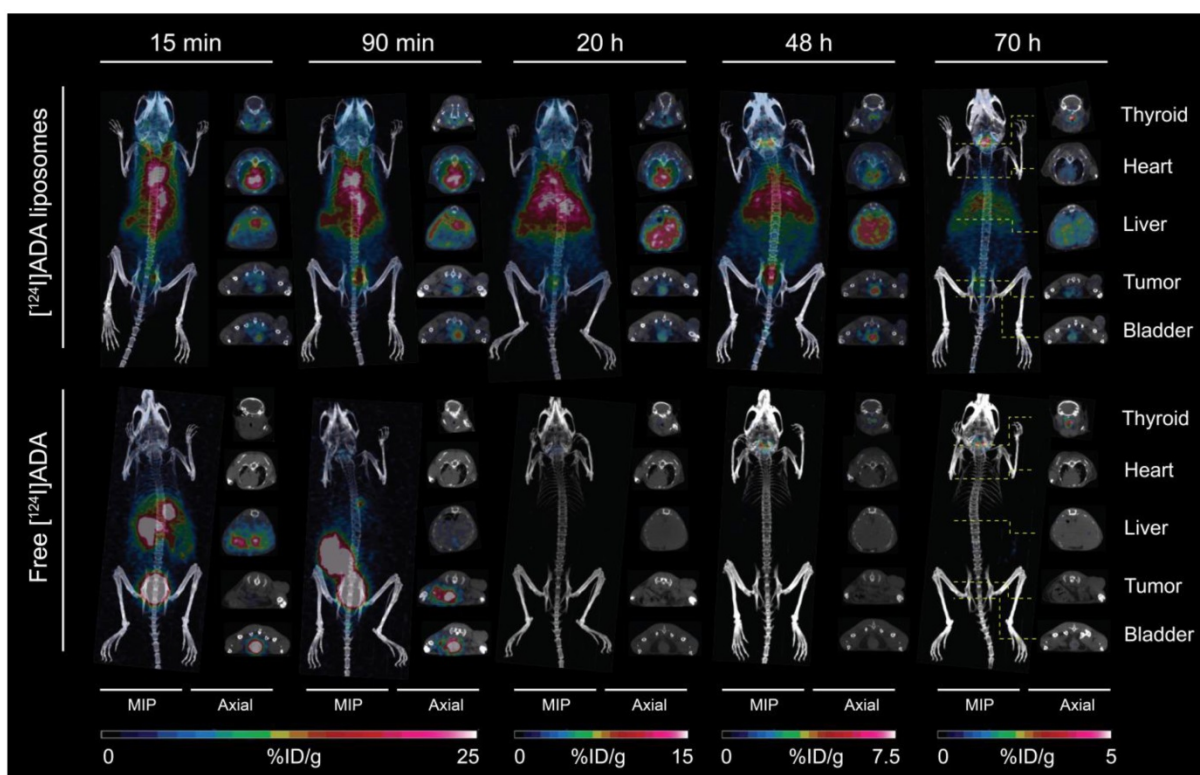
Figure 4. MIP and axial PET/CT images of systemically administered free [124I]ADA and [124I]ADA-loaded liposomes in CT26 tumor-bearing mice at 15 min, 90 min 20 h, 48 h and 70 h pi. The position of the axial image projections is illustrated for the 70 h timepoint using yellow dotted lines.

For free [124I]ADA, rapid blood clearance (**Figure 5A**) and urinary excretion during the first 15 min were observed (**Figure 5E**). Rapid clearance of free [124I]ADA from the spleen, liver and kidney, and low tumor activity was also observed (**Figure 5B-C**), reflecting the rapid clearance of free [124I]ADA from the blood pool within these organs. [124I]ADA thus exhibits the typical renal clearance of small, polar substances. After 72 h, a total retention of 0.015 %ID was determined in the thyroid by well counting (**Figure 5F**). Assuming a thyroid weight of 11 mg [48], this corresponds to 1.4 %ID/g accumulation in the thyroid of the non-liposomal [124I]ADA. This is likely to be a result of the bulk of the radioactivity clearing from the organism before appreciable deiodination of [124I]ADA has occurred. The limited thyroid accumulation indicates that the compound is relatively stable *in vivo*. In comparison, administration of free 131I- in rats resulted in 270 %ID/g accumulation in the thyroid after 6 h [49].

Contrary to the free compound, [124I]ADA-loaded liposomes circulated with a half-life of 19.7 h, when estimated by a mono-exponential fit of data collected during 0-72 h (R^2 = 0.98). At the first PET scan (t = 15 min), 29.3 %ID/g, 12.0 %ID/g and 10.8 %ID/g were found in the blood, liver and spleen respectively, accounting for approximately 74% of the total activity when assuming organ/blood weight

percentages (%w/w) of 8.5%, 4.9% and 0.54% for blood, liver and spleen [50] and a 23 g average body weight of the BALB/c mice. The circulating half-life of the [124I]ADA-loaded liposomes is comparable to earlier reports for liposomal CT contrast agents [27] and for liposomes carrying 64Cu- and 52Mn-radiolabels that are known to be stable *in vivo* [5,11,15,17,51]. This, as well as the minimal radioactivity in the urinary bladder, which could be either in the form of [124I]ADA or breakdown products, (**Figure 5E**) substantiate that the stealth liposomes entrapping [124I]ADA are stable during circulation in the blood. Liver, spleen and kidneys also displayed the expected activity of liposomal [124I]ADA, which corresponds with previous reports on comparable nanoparticles. The highest activity was observed at 1.5 h post injection (pi.) for these organs, which contradicts earlier reports on long-circulating liposomes where the maximal accumulation typically occurred after 12-40 h [10,17]. This indicates that radioactivity was able to leave these organs during the imaging period, which is not expected to occur if [124I]ADA is maintained within the stealth liposome. The tumor-to-blood ratio, shown in **Figure 5D**, increases as a function of time for the liposomal [124I]ADA, further indicating that the extravascular activity in this region increases with respect to the intravascular as a result of EPR-dependent liposome

accumulation. Previous biodistribution studies of stealth liposomes have proven these to be very stable in circulation [5,17,51], which suggests that free [124I]ADA or breakdown products were released from the liposomes after accumulation. The absence of a precipitate in the cryo-TEM images (**Figure 2D-E**) lends support to this hypothesis, as formation of crystalized [124I]ADA inside the liposomes would have been likely to slow down the release kinetics [52]. This release may be a result of uptake and digestion of the liposomes by resident immune cells, or loss of the trans-membrane pH-gradient. The latter possibility was previously suggested as a reason for unloading of liposomal doxorubicin [53]. *In vitro* studies by Forster et al. and Mayer et al. showed that the pH gradient of liposomes composed of EPC or DPPC may dissipate over time when incubated at 37 °C in buffer or serum, which supports our hypothesis that [124I]ADA may have leaked from the liposomes after they had accumulated [43,54]. Since higher thyroid accumulation was observed for the liposomal [124I]ADA (1.06 %ID/thyroid, 96 %ID/g assuming a thyroid weight of 11 mg [48], **Figure 5F**) compared to freely administered [124I]ADA, the compound is probably released from the organs of uptake, with subsequent renal excretion and only limited

deiodination, as thyroid entrapment of free iodine would have been more pronounced. In comparison, Ke and coworkers reported a 12-fold higher thyroid accumulation (12.9 %ID/thyroid) for euthyroid mice upon administration of 131I [55].

The stability of [*I]ADA was further investigated *in vitro* to shed light on the possible deiodination of the compound (**Figure S7**). In this test assay, the radiolabeled compound was incubated at 37 °C with mouse serum (50%), mouse liver homogenate in PBS and neat PBS as control, and the mixtures were monitored by radio-TLC for 3 days. Liver homogenate was included as a test for deiodination, due to the high presence of deiodinases in this organ. No breakdown was observed in PBS, whereas about 5% [*I]ADA was degraded after 3 days in serum and about 10% in the liver homogenate. Multiple metabolites were observed, suggesting that other pathways of degradation besides deiodination took place. That degradation was slightly more pronounced in the liver homogenate may be a result of deiodination occurring. In general, however, the compound exhibited good stability in both biological samples, which is also supported by the relatively limited thyroid accumulation of radioiodine observed *in vivo*.
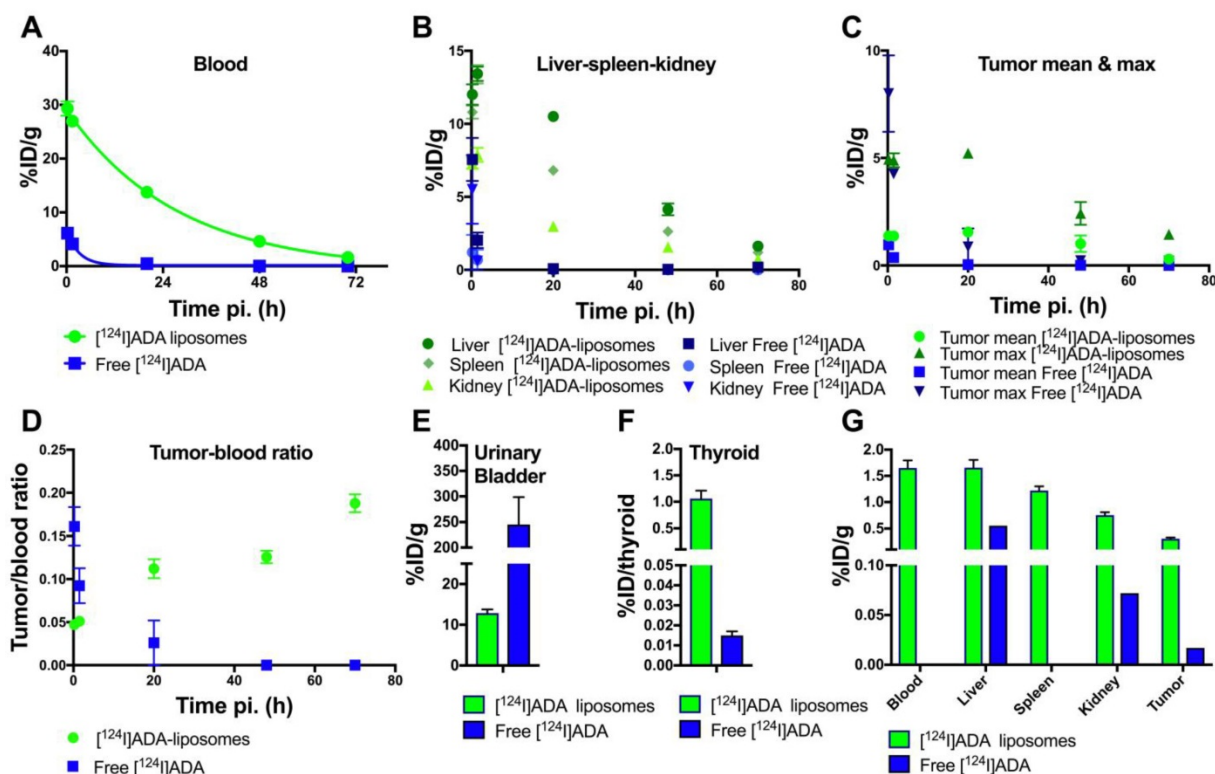

Figure 5. PET-derived biodistribution of free [124I]ADA and [124I]ADA loaded liposomes. **(A-E)** The accumulation of free [124I]ADA (n = 3) and [124I]ADA-loaded liposomes (n = 5) in (A) blood, (B) liver, kidney and spleen, (C) tumor, and (D) tumor-to-blood ratio are shown as a function of time post injection (pi.). The radioactivity in the urinary bladder (E) was measured 15 min post injection. The results are presented as mean ± SEM for all organs and blood, whereas the tumor is given as both mean ± SEM and max ± SEM. **(F-G)** Ex vivo biodistribution data, 72 h post injection, of free [124I]ADA (n = 3) and [124I]ADA-loaded liposomes (n = 5), based on organ well counting. The data are presented as mean ± SEM. The thyroid uptake is expressed as %ID ± SEM per thyroid.

The low short-term degradation and deiodination of the [*I]ADA compound observed *in vitro* further supports the low thyroid accumulation observed for [124I]ADA administered in HEPES. The longer blood circulation, higher liver accumulation, and the more pronounced *in vitro* degradation of [124I]ADA incubated in liver homogenate also supports the 70-fold higher thyroid accumulation for the liposomal [124I]ADA compared to free [124I]ADA (**Figure 5F**). Partially lipophilic drugs, like [124I]ADA, are expected to be taken up in hepatocytes and possibly undergo enzymatic modifications, which may explain the higher thyroid accumulation for the liposomal [124I]ADA. Liposomes are, on the other hand, expected to be taken up in the liver by resident Kupffer cells. Further studies are needed to decipher the histological distribution of [124I]ADA and its consequences for release and deiodination. The mean tumor accumulation of 1.5 %ID/g (**Figure 5C**) is likewise lower than the 4-6 %ID/g normally reported for CT26 tumor-bearing mice after accumulation for 24 h [17], which suggests that 124I leaves the tumor in an undetermined form. The potential indication of a continuous release of 124I in some chemical form, possibly [124I]ADA, could bias our calculated half-life for [124I]ADA-liposomes in circulation. Considering the high blood radioactivity observed, this is only of minor concern following the observed rapid urinary excretion of [124I]ADA when administered in its free form.

The procedure for radiolabeling liposomes with radioiodine presented here involves an early radiolabeling step, giving a radiolabeled small molecule that is subsequently purified and loaded into liposomes. This mirrors previous procedures, such as the use of the Bolton-Hunter reagent [32] as well as the use of radiolabeled prosthetic groups. For a clinically used radiopharmaceutical this is a disadvantage due to the increased handling of radioactive material. This could potentially be limited by automation. In the case at hand, this could involve the initial radiolabeling happening in a vessel containing $CuSO_4$ and the substrate, to which AcOH and the radioiodine could be added, followed by heating. Automated Sep-Pak purification would benefit from a fixed aq. NH_4OH concentration in the eluting medium, which is likely to be possible. To the dried compound, the liposome dispersion would simply be added and heated to effectuate loading. To avoid size exclusion chromatography, an improved Sep-Pak purification step would be beneficial to reduce radioactive impurities to below 5%. As the loading itself is quantitative, this would likely give a sufficiently radiochemically pure product.

Despite the potential concern of using [124I]ADA-liposomes as imaging agents to determine the maximum accumulation levels of liposomes in tumors and their biodistribution over extended periods, the observations in the present study are highly encouraging towards developing liposomes for therapeutic use. The prolonged retention in and slow release of drugs from liposomes is a potential Achilles heel for liposomal delivery of anti-cancer drugs. The [124I]ADA-liposomes display a continuous relatively stable activity level in tumors and this indicates that their content of [124I]ADA is continuously released at a rate high enough to equilibrate their EPR-dependent accumulation. New classes of anti-cancer therapeutics or pro-drugs, etc. constructed with chemical characteristics comparable to [124I]ADA may therefore prove beneficial to avoid slow release kinetics and become directly available to cells within the tumors.

Conclusion

We introduced a versatile technique to formulate radioiodine in liposomes in quantitative encapsulation yields. This was achieved by radioiodination of a membrane-crossing compound, [124I]ADA, that was remote loaded by an ion gradient. The loaded radioiodinated species was found to be stably encapsulated in circulation, as well as *in vitro*. *In vivo*, however, evidence of release of the radioiodine was observed after uptake in organs such as liver and spleen as well as tumor. This observation is highly encouraging for the future development and construction of liposomal anti-cancer drugs, as drugs with compatible chemical characteristics as ADA may provide means to overcome the problematic entrapment stability of liposomes and subsequent slow release kinetics of chemotherapeutics.

Abbreviations

ADA: amino diatrizoic acid; CT: computed tomography; EPR: enhanced permeation and retention; ID: injected dose; LUV: large unilamellar vesicle; MIP: maximal intensity projection; MRI: magnetic resonance imaging; NMR: nuclear magnetic resonance; PEG: polyethylene glycol; PET: positron emission tomography; ROI: region of interest; SPECT: single photon emission computed tomography; TLC: thin-layer chromatography.

Supplementary Material

Supplementary figures.
http://www.thno.org/v08p5828s1.pdf

Acknowledgements

We acknowledge the Core Facility for Integrated Microscopy, Faculty of Health and Medical Sciences, University of Copenhagen.

Competing Interests

The authors have declared that no competing interest exists.

References

1. Ehlerding EB, Grodzinski P, Cai W, Liu CH. Big Potential from Small Agents: Nanoparticles for Imaging-Based Companion Diagnostics. ACS Nano. 2018; 12: 2106–2121.

2. Gaddy DF, Lee H, Zheng J, Jaffray DA, Wickham TJ, Hendriks BS. Dosimetric Evaluations of 64 Cu-Loaded HER2 / ErbB2- Targeted Liposomal Doxorubicin (64 Cu-MM-302) in Rodents and Primates. EJNMMI Res. 2015; 5: 1–10.

3. Jadvar H, Chen X, Cai W, Mahmood U. Radiotheranostics in Cancer Diagnosis and Management. Radiology. 2018; 286: 388–400.

4. Desser TS, Rubin DL, Muller H, McIntire GL, Bacon ER, Toner JL. Blood Pool and Liver Enhancement in CT with Liposomal Lodixanol: Comparison with Lohexol. Acad Radiol. 1999; 6: 176–183.

5. Hansen AE, Petersen AL, Henriksen JR, Boerresen B, Rasmussen P, Elema DR, Rosenschoeld PM, Kristensen AT, Kjær A, Andresen TL, et al. Positron Emission Tomography Based Elucidation of the Enhanced Permeability and Retention Effect in Dogs with Cancer Using Copper-64 Liposomes. ACS Nano. 2015; 9: 6985–6995.

6. Lee H, Shields AF, Siegel BA, Miller KD, Krop I, Ma CX, Lorusso PM, Munster PN, Campbell K, Gaddy DF, et al. 64Cu-MM-302 Positron Emission Tomography Quantifies Variability of Enhanced Permeability and Retention of Nanoparticles in Relation to Treatment Response in Patients with Metastatic Breast Cancer. Clin Cancer Res. 2017; 23: 4190–4202.

7. Frellsen AF, Hansen AE, Jølck RI, Kempen PJ, Severin GW, Rasmussen PH, Kjær A, Jensen ATI, Andresen TL. Mouse Positron Emission Tomography Study of the Biodistribution of Gold Nanoparticles with Different Surface Coatings Using Embedded Copper-64. ACS Nano. 2016; 10: 9887–9898.

8. Pérez-Medina C, Abdel-Atti D, Tang J, Zhao Y, Fayad ZA, Lewis JS, Mulder WJM, Reiner T. Nanoreporter PET Predicts the Efficacy of Anti-Cancer Nanotherapy. Nat Commun. 2016; 7: 1–8.

9. Kulkarni A, Rao P, Natarajan S, Goldman A, Sabbisetti VS, Khater Y, Korimerla N, Chandrasekar V, Mashelkar RA, Sengupta S. Reporter Nanoparticle That Monitors Its Anticancer Efficacy in Real Time. Proc Natl Acad Sci. 2016; 113: E2104–E2113.

10. Edmonds S, Volpe A, Shmeeda H, Parente-Pereira AC, Radia R, Baguña-Torres J, Szanda I, Severin GW, Livieratos L, Blower PJ, et al. Exploiting the Metal-Chelating Properties of the Drug Cargo for in Vivo Positron Emission Tomography Imaging of Liposomal Nanomedicines. ACS Nano. 2016; 10: 10294–10307.

11. Seo JW, Mahakian LM, Kheirolomoom A, Zhang H, Meares CF, Ferdani R, Anderson CJ, Ferrara KW. Liposomal Cu-64 Labeling Method Using Bifunctional Chelators: Poly(Ethylene Glycol) Spacer and Chelator Effects. Bioconjug Chem. 2010; 21: 1206–1215.

12. Louie A. Multimodality Imaging Probes: Design and Challenges. Chem Rev A. 2010; 110: 3146–3195.

13. Bao A, Goins B, Klipper R, Negrete G, Phillips WT. Direct Tc-99m Labeling of Pegylated Liposomal Doxorubicin (Doxil) for Pharmacokinetic and Non-Invasive Imaging Studies. Pharmacology. 2004; 308: 419–425.

14. Wang HE, Yu HM, Lu YC, Heish NN, Tseng YL, Huang KL, Chuang KT, Chen CH, Hwang JJ, Lin WJ, et al. Internal Radiotherapy and Dosimetric Study for 111In/177Lu-Pegylated Liposomes Conjugates in Tumor-Bearing Mice. Nucl. Instruments Methods Phys. Res. Sect. A Accel. Spectrometers, Detect. Assoc. Equip. 2006; 569: 533–537.

15. Henriksen JR, Petersen AL, Hansen AE, Frankær CG, Harris P, Elema DR, Kristensen AT, Kjær A, Andresen TL. Remote Loading of 64Cu2+ into Liposomes without the Use of Ion Transport Enhancers. ACS Appl Mater Interfaces. 2015; 7: 22796–22806.

16. Seo JW, Mahakian LM, Tam S, Qin S, Ingham ES, Meares CF, Ferrara KW. The Pharmacokinetics of Zr-89 Labeled Liposomes over Extended Periods in a Murine Tumor Model. Nucl Med Biol. 2015; 42: 155–163.

17. Jensen AI, Severin GW, Hansen AE, Fliedner FP, Eliasen R, Parhamifar L, Kjær A, Andresen TL, Henriksen JR. Remote-Loading of Liposomes with Manganese-52 and in Vivo Evaluation of the Stabilities of 52Mn-DOTA and 64Cu-DOTA Using Radiolabelled Liposomes and PET Imaging. J Control Release. 2018; 269: 100–109.

18. Sachse A. Iodinated Liposomes as Contrast Agents. In: Bulte JWM, Modo MMJ Ed. Nanoparticles in Biomedical Imaging. New York: Springer; 2007: 371-410.

19. Jensen ATI, Binderup T, Andresen TL, Kjær A, Rasmussen PH. PET Imaging of Liposomes Labeled with an [18F]-Fluorocholesteryl Ether Probe Prepared by Automated Radiosynthesis. J Liposome Res. 2012; 22: 295–305.

20. Dissanayake S, Dissanayake D, Taylor DB. Radio-Guided Occult Lesion Localisation Using Iodine 125 Seeds "ROLLIS" to Guide Surgical Removal of an Impalpable Posterior Chest Wall Melanoma Metastasis. J Med Radiat Sci. 2015; 62: 230–233.

21. Schaarup-Jensen H, Jensen AI, Hansen AE, El Ali HH, Hammershøj P, Jølck RI, Kjær A, Andresen TL, Clausen MH. Injectable Iodine-125 Labeled Tissue Marker for Radioactive Localization of Non-Palpable Breast Lesions. Acta Biomater. 2018; 65: 197–202.

22. Thisgaard H, Halle B, Aaberg-Jessen C, Olsen BB, Therkelsen ASN, Dam JH, Langkjaer N, Munthe S, Någren K, Høilund-Carlsen PF, et al. Highly Effective Auger-Electron Therapy in an Orthotopic Glioblastoma Xenograft Model Using Convection-Enhanced Delivery. Theranostics. 2016; 6: 2278–2291.

23. Mahajan S, Divgi CR. The Role of Iodine-124 Positron Emission Tomography in Molecular Imaging. Clin Transl Imaging. 2016; 4: 297–306.

24. Gulec SA, Kuker RA, Goryawala M, Fernandez C, Perez R, Khan-Ghany A, Apaza A, Harja E, Harrell M. [124] I PET/CT in Patients with Differentiated Thyroid Cancer: Clinical and Quantitative Image Analysis. Thyroid 2016; 26: 441–448.

25. Koehler L, Gagnon K, McQuarrie S, Wuest F. Iodine-124: A Promising Positron Emitter for Organic PET Chemistry. Molecules 2010; 15: 2686–2718.

26. Elrod DB, Partha R, Danila D, Casscells SW, Conyers JL. An Iodinated Liposomal Computed Tomographic Contrast Agent Prepared from a Diiodophosphatidylcholine Lipid. Nanomedicine Nanotechnology, Biol Med 2009; 5: 42–45.

27. Zheng J, Liu J, Dunne M, Jaffray DA, Allen C. In Vivo Performance of a Liposomal Vascular Contrast Agent for CT and MR-Based Image Guidance Applications. Pharm Res. 2007; 24: 1193–1201.

28. Sachse A, Leike JU, Schneider T, Wagner SE, Rössling GL, Krause W, Brandl M. Biodistribution and CT Blood Pool Imaging Properties of PEG Coated Iopromide Carrying Liposomes. Investig Radiol. 1997; 32: 44–50.

29. Leike JU, Sachse A, Rupp K. Characterization of Continuously Extruded Iopromide-Carrying Liposomes for Computed Tomography Blood-Pool Imaging. Invest Radiol. 2001; 36: 303–308.

30. Kao C, Hoffman EA, Beck KC, Bellamkonda R V, Annapragada A V. Iohexol for X-Ray – Based Blood Pool Imaging. Acad Radiol. 2003; 10: 475–483.

31. Mukundan S, Ghaghada KB, Badea CT, Kao CY, Hedlund LW, Provenzale JM, Johnson GA, Chen E, Bellamkonda R V., Annapragada A. A Liposomal Nanoscale Contrast Agent for Preclinical CT in Mice. Am J Roentgenol. 2006; 186: 300–307.

32. Mougin-Degraef M, Jestin E, Bruel D, Remaud-Le Saëc P, Morandeau L, Faivre-Chauvet A, Barbet J. High-Activity Radio-Iodine Labeling of Conventional and Stealth Liposomes. J Liposome Res. 2006; 16: 91–102.

33. Madden TD, Harrigan PR, Tai LCL, Bally MB, Mayer LD, Redelmeier TE, Loughrey HC, Tilcock CPS, Reinish LW, Cullis PR. The Accumulation of Drugs within Large Unilamellar Vesicles Exhibiting a Proton Gradient: A Survey. Chem Phys Lipids. 1990; 53: 37–46.

34. Haran G, Cohen R, Bar LK, Barenholz Y. Transmembrane Ammonium Sulfate Gradients in Liposomes Produce Efficient and Stable Entrapment of Amphipathic Weak Bases. Biochim. Biophys Acta. 1993; 1151: 201–215.

35. Harrigan PR, Wong KF, Redelmeier TE, Wheeler JJ, Cullis PR. Accumulation of Doxorubicin and Other Lipophilic Amines into Large Unilamellar Vesicles in Response to Transmembrane PH Gradients. Biochim Biophys Acta. 1993; 1149: 329–338.

36. Fritze A, Hens F, Kimpfler A, Schubert R, Peschka-Süss R. Remote Loading of Doxorubicin into Liposomes Driven by a Transmembrane Phosphate Gradient. Biochim. Biochim Biophys Acta. 2006; 1758: 1633–1640.

37. Bao A, Goins B, Klipper R, Negrete G, Phillips WT. 186Re-Liposome Labeling Using 186Re-SNS/S Complexes : In Vitro Stability , Imaging , and Biodistribution in Rats. J Nucl Med. 2003; 44: 1992–2000.

38. Bao A, Phillips WT, Goins B, Zheng X, Sabour S, Natarajan M, Ross Woolley F, Zavaleta C, Otto RA. Potential Use of Drug Carried-Liposomes for Cancer Therapy via Direct Intratumoral Injection. Int J Pharm. 2006; 316: 162–169.

39. Phillips WT, Goins B, Bao A, Vargas D, Guttierez JE, Trevino A, Miller JR, Henry J, Zuniga R, Vecil G, et al. For Treatment of Glioblastoma. Neuro Oncol. 2012; 14: 416–425.

40. Hong SS, Kim AY, Kwon SB, Kim PN, Lee MG, Ha HK. Three-Dimensional CT Enterography Using Oral Gastrografin in Patients with Small Bowel Obstruction: Comparison with Axial CT Images or Fluoroscopic Findings. Abdom Imaging. 2010; 35: 556–562.

41. J.R. H, L.A. H, K.J. C. Myocardial Ischemia during Intravenous DSA in Patients with Cardiac Disease. Radiology. 1984; 153: 577–582.

42. El Aissi R, Liu J, Besse S, Canitrot D, Chavignon O, Chezal JM, Miot-Noirault E, Moreau E. Synthesis and Biological Evaluation of New Quinoxaline Derivatives of ICF01012 as Melanoma-Targeting Probes. ACS Med Chem Lett. 2014; 5: 468–473.

43. Forster V, Luciani P, Leroux JC. Treatment of Calcium Channel Blocker-Induced Cardiovascular Toxicity with Drug Scavenging Liposomes. Biomaterials. 2012; 33: 3578–3585.

44. Čeh B, Lasic DD. A Rigorous Theory of Remote Loading of Drugs into Liposomes: Transmembrane Potential and Induced PH-Gradient Loading and Leakage of Liposomes. J Colloid Interface Sci. 1995; 22: 9–18.

45. Litzinger DC, Buiting AMJ, van Rooijen N, Huang L. Effect of Liposome Size on the Circulation Time and Intraorgan Distribution of Amphipathic Poly(Ethylene Glycol)-Containing Liposomes. Biochim Biophys Acta 1994; 1190: 99–107.

46. Cullis PR, Hope MJ, Bally MB, Madden TD, Mayer LD, Fenske DB. Influence of PH Gradients on the Transbilayer Transport of Drugs , Lipids , Peptides and Metal Ions into Large Unilamellar Vesicles. Biochim Biophys Acta 1997; 1331: 187–211.
47. Li X, Hirsh DJ, Cabral-Lilly D, Zirkel A, Gruner SM, Janoff AS, Perkins WR. Doxorubicin Physical State in Solution and inside Liposomes Loaded via a PH Gradient. Biochim Biophys Acta 1998; 1415: 23–40.
48. Krinke GJ. Normative Histology of Organs. In: Hedrich H, Bullock G Ed. The Laboratory Mouse, 1st ed. Cambridge Massachusetts: Academic Press; 2004: 133–165
49. Spetz J, Rudqvist N, Forssell-Aronsson E. Biodistribution and Dosimetry of Free ^{211}At, ^{125}I $^-$ and ^{131}I $^-$ in Rats. Cancer Biother Radiopharm. 2013; 28: 657–664.
50. Cook MJ. Anatomy. In: Foster H, Small J, Fox J Ed. The mouse in biomedical research, 1st ed. Cambridge Massachusetts: Academic Press; 1983: 101–120
51. Jai WS, Zhang H, Kukis DL, Meares CF, Ferrara KW. A Novel Method to Label Preformed Liposomes with 64Cu for Positron Emission Tomography (PET) Imaging. Bioconjug Chem. 2008; 19: 2577–2584.
52. Russell LM, Hultz M, Searson PC. Leakage Kinetics of the Liposomal Chemotherapeutic Agent Doxil: The Role of Dissolution, Protonation, and Passive Transport, and Implications for Mechanism of Action. J Control Release 2018; 269: 171–176.
53. Lee RJ, Wang S, Turk MJ, Low PS. The Effects of PH and Intraliposomal Buffer Strength on the Rate of Liposome Content Release and Intracellular Drug Delivery. Biosci Rep. 1998; 18: 69–78.
54. Mayer LD, Reamer J, Bally MB. Intravenous Pretreatment with Empty PH Gradient Liposomes Alters the Pharmacokinetics and Toxicity of Doxorubicin through in Vivo Active Drug Encapsulation. J Pharm Sci. 1999; 88: 96–102.
55. Ke CC, He ZM, Hsieh YJ, Huang CW, Li JJ, Hwu L, Chen YA, Yang BH, Chang CW, Huang WS, et al. Quantitative Measurement of the Thyroid Uptake Function of Mouse by Cerenkov Luminescence Imaging. Sci Rep. 2017; 7: 1–7.